The role of air-sea fluxes in Subantarctic Mode Water formation

James W. Holte,[1] Lynne D. Talley,[2] Teresa K. Chereskin,[2] and Bernadette M. Sloyan[3,4]

[1]   Two hydrographic surveys and a one-dimensional mixed layer model are used to assess the role of air-sea fluxes in forming deep Subantarctic Mode Water (SAMW) mixed layers in the southeast Pacific Ocean. Forty-two SAMW mixed layers deeper than 400 m were observed north of the Subantarctic Front during the 2005 winter cruise, with the deepest mixed layers reaching 550 m. The densest, coldest, and freshest mixed layers were found in the cruise's eastern sections near 77°W. The deep SAMW mixed layers were observed concurrently with surface ocean heat loss of approximately -200 W m^{-2}. The heat, momentum, and precipitation flux fields of five flux products are used to force a one-dimensional KPP mixed layer model initialized with profiles from the 2006 summer cruise. The simulated winter mixed layers generated by all of the forcing products resemble Argo observations of SAMW; this agreement also validates the flux products. Mixing driven by buoyancy loss and wind forcing is strong enough to deepen the SAMW layers. Wind-driven mixing is central to SAMW formation, as model runs forced with buoyancy forcing alone produce shallow mixed layers. Air-sea fluxes indirectly influence winter SAMW properties by controlling how deeply the profiles mix. The stratification and heat content of the initial profiles determine the properties of the SAMW and the likelihood of deep mixing. Summer profiles from just upstream of Drake Passage have less heat stored between 100 and 600 m than upstream profiles, and so, with sufficiently strong winter forcing, form a cold, dense variety of SAMW.

1.   Introduction

[2]   The deepest mixed layers in the Southern Ocean are found equatorward of the Subantarctic Front (SAF), the northernmost front of the Antarctic Circumpolar Current (ACC). Termed Subantarctic Mode Water (SAMW) by *McCartney* [1977], the waters enclosed in the deeply-mixed region are characterized by a potential vorticity minimum and an oxygen maximum. The warmest SAMW is found in the South Atlantic and western Indian Oceans. The densest, coolest, and freshest SAMW is formed in the southeast Pacific Ocean just before the ACC enters Drake Passage [*McCartney*, 1977; *Talley*, 1996; *Hanawa and Talley*, 2001]. *McCartney* [1977] attributed the observed eastward freshening and cooling of SAMW from south of Africa to Drake Passage to the cumulative effects of air-sea fluxes of precipitation and heat.

[3]   SAMW is important to many global-scale processes. The formation of thick mode and intermediate water masses is a primary mechanism for sequestering anthropogenic CO_2 in the ocean interior [*Sabine et al.*, 2002]. SAMW forms the upper limb of the global overturning circulation [*Sloyan and Rintoul*, 2001] and renews the waters of the lower thermocline in the subtropical gyres [*McCartney*, 1982]. The heat, freshwater, and carbon transports associated with SAMW's global-scale circulation confirm its relevance to studies of the Earth's climate and of the ocean's global overturning circulation [*Keeling and Stephens*, 2001; *Pahnke and Zahn*, 2005].

[4]   Because of its importance to climate, many recent studies have investigated SAMW variability. The Southern Ocean's mid-depth warming is well documented, especially near the ACC [*Gille*, 2002]. In the Pacific sector of the Southern Ocean, SAMW has warmed and freshened [*Wong et al.*, 2001; *Bryden et al.*, 2003], and this observed freshening may be attributed to anthropogenic climate change [*Banks et al.*, 2000]. *Naveira-Garabato et al.* [2009] examined the interdecadal variability of SAMW in Drake Passage and determined that the variability was primarily due to modes of Southern Hemisphere climate variability, such as the Southern Annular Mode and El Niño–Southern Oscillation.

[5]   As noted by *Rintoul and England* [2002], the implications of the observed variability of SAMW are difficult to deduce without knowledge of the formation mechanisms.

---

[1]Woods Hole Oceanographic Institution, Woods Hole, Massachusetts, USA.
[2]Scripps Institution of Oceanography, University of California, San Diego, La Jolla, California, USA.
[3]Center for Australian Weather and Climate Research, CSIRO Marine and Atmospheric Research, Hobart, Tasmania, Australia.
[4]Wealth from Oceans National Research Flagship, CSIRO, Hobart, Tasmania, Australia.

Many processes contribute to SAMW formation: gyre inflow, cross-frontal advection in the form of Ekman transport, eddies, and intrusions; heat and freshwater fluxes at the air-sea interface and at the base of the mixed layer; and mixing (Figure 1). The relative contributions of these mechanisms to SAMW formation are the topic of frequent study.

[6] Many papers have focused on air-sea fluxes and Ekman transport, which transports cold, fresh polar waters across the SAF into the SAMW formation region. *Speer et al.* [2000] and *Sloyan and Rintoul* [2001] found that air-sea fluxes alone could not account for the observed temporal variability of SAMW properties, and attributed the variability to Ekman transport. *Naveira-Garabato et al.* [2009] found that the interannual variability of SAMW and Antarctic Intermediate Water (AAIW) in Drake Passage was primarily driven by variations in wintertime heat fluxes and net evaporation, which were modulated by the El Niño–Southern Oscillation; Ekman transport dominated SAMW ventilation for short periods. *Vivier et al.* [2010] found that anomalous air-sea heat flux was the dominant driver of non-seasonal temperature anomalies over most of the Southern Ocean, but that anomalous Ekman heat fluxes accounted for 20% to 40% of the temperature variance in the latitude band of SAMW formation.

[7] Eddies have been shown to modify Ekman transport and air-sea fluxes [*Sallée et al.*, 2008] and to influence SAMW property variability [*Herraiz-Borreguero and Rintoul*, 2010]. *Hogg et al.* [2008] used an eddy-resolving quasi-geostrophic model of the Southern Ocean to show that the poleward eddy heat flux has a larger effect on SSTs than equatorward Ekman transport. *Sallée et al.* [2008] found that in specific regions, particularly the western Indian and western Pacific, eddy heating counterbalanced cooling due to Ekman transport.

[8] Besides driving Ekman transport, wind energy input to the ocean drives considerable mixing at and below the base of the mixed layer in the SAMW formation region [*Sloyan et al.*, 2010]. Using an ocean general circulation model, *Kamenkovich* [2005] found that daily fluctuations in the momentum flux had a larger effect on the time-mean temperature and mixed layer structure than the heat flux. *Park and Gambéroni* [1997], in the Indian Ocean, found that cross-frontal intrusions, which could transport polar water across the SAF, were not continuous in time and space, but occurred impulsively and were associated with meanders and eddies in the ACC. *Chereskin et al.* [2010] have shown that SAF meanders in the region upstream of Drake Passage are quasi-stationary on seasonal time scales; the deep SAMW mixed layers therefore maintain their position relative to the front during their winter formation.

[9] This paper is part one of a two-part study looking at the contributions of air-sea fluxes and cross-frontal exchange to SAMW formation in the southeast Pacific. Our study is based on hydrographic and air-sea flux observations from two cruises in the southeast Pacific Ocean. The first cruise, in austral winter, observed the deep winter SAMW mixed layers. The second cruise, in austral summer, observed their subsequent restratification.

[10] In part one, we focus on how air-sea forcing, initial profile stratification, and vertical mixing determine the SAMW mixed layers' depths, properties, area extent, relationship to the SAF, and downstream variation. During the cruise, the deep SAMW mixed layers north of the SAF were observed concurrently with strong air-sea forcing. Five flux products were compared to the cruise fluxes, and then used to force a one-dimensional K-Profile Parameterization (KPP) mixed layer model [*Large et al.*, 1994] initialized with profiles from the 2006 austral summer cruise. We temporarily neglect any advective mechanisms and consider SAMW formation as a one-dimensional process to isolate the importance of air-sea fluxes to SAMW formation. The simulated winter mixed layers generated by all of the forcing products resemble Argo observations of SAMW in the southeast Pacific. However, the simulated SAMW mixed layers evolved by NCEP most closely resembled Argo's SAMW observations. A series of model runs with idealized forcing provide insight into the importance of wind-driven mixing, initial profile, and air-sea forcing strength to SAMW formation and the distribution of SAMW properties.

[11] In part two (J. Holte et al., Optimum multiparameter analysis of cross-frontal exchange at the Subantarctic Front, manuscript in preparation, 2012) we evaluate the importance of cross-frontal exchange to SAMW formation. Numerous instances of cross-frontal exchange were observed during the two cruises, including sub-surface intrusions penetrating north of the SAF, cold-core eddies in the SAMW formation region, and a pattern of low mixed layer salinity in the SAMW formation region during the 2006 austral summer cruise that is suggestive of Ekman transport. We use an optimum multiparameter (OMP) analysis to estimate the cross-frontal exchange between the 27.0 and 27.3 kg m^{-3} isopycnals. This isopycnal range is generally below the mixed layer, and so is not locally forced by air-sea fluxes or wind-driven mixing. The OMP analysis reveals that the fractional content of Polar Frontal Zone (PFZ) water north of the SAF increases by approximately 10% for every 15° of longitude. A simple bulk calculation reveals that this magnitude of cross-frontal exchange could cause the along-front freshening and cooling of the SAMW mixed layers observed by Argo.

[12] This paper is organized as follows. Section 2 describes the data collected during the two cruises. Section 3 summarizes the 2005 austral winter cruise SAMW mixed layer observations. The cruise heat flux measurements are outlined in section 4 and used to evaluate various model and observation-derived heat flux products in section 5. The flux products are then used to force a one-dimensional mixed layer model to test how air-sea fluxes contribute to the deep mixed layers. The model runs are initialized with profiles from the 2006 austral summer cruise and evolved with the flux products for one year beginning at their collection time. The simulated winter mixed layers, taken as the August mean of each model run, are compared to profiles from the 2005 austral winter cruise and Argo. Section 6 contains the mixed layer modeling results and analysis. Section 7 discusses the results of three model runs with altered NCEP forcing. Section 8 examines the importance of initial profiles in SAMW formation. Section 9 summarizes and discusses the results.

2. Data

[13] Two hydrographic surveys conducted on R/V *Knorr* in the southeast Pacific Ocean provide high quality, synoptic observations of the SAMW formation region during winter
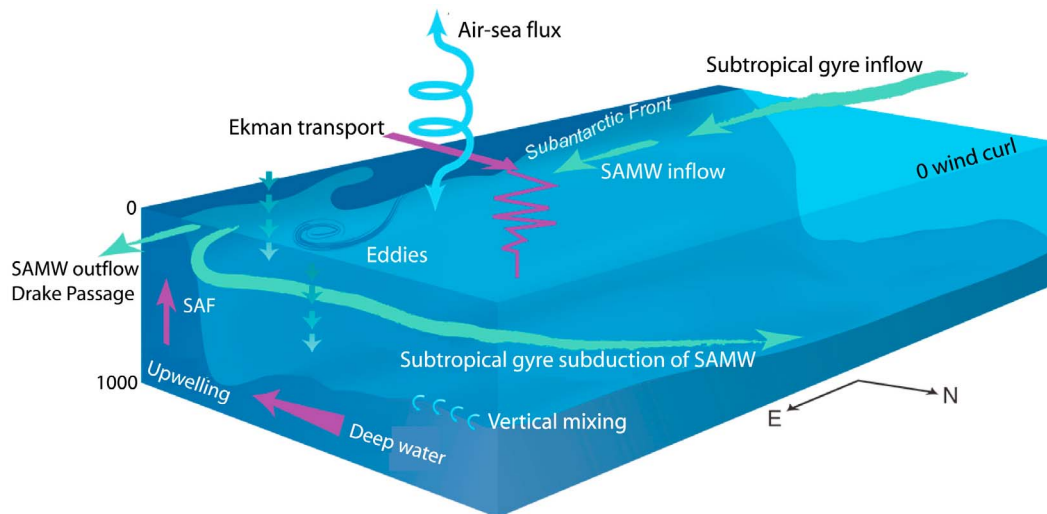
Figure 1. Schematic of the various processes that contribute to SAMW formation in the southeastern Pacific Ocean. SAMW is exported to the gyre and through Drake Passage.

and summer (Figure 2). The first cruise, from August 23 to October 5, 2005, observed the deep winter mixed layers. The second, from January 30 to March 14, 2006, observed the subsequent restratification. Both cruises departed from Punta Arenas, followed a sawtooth path out to 103°W, and concluded near Puerto Montt, crossing the SAF six times. CTD station spacing was approximately 50 km. Each cruise included two diamond-patterned intensive surveys, one in the SAMW formation region and another at the SAF; the location of these surveys varied by cruise depending on the position of the SAF.
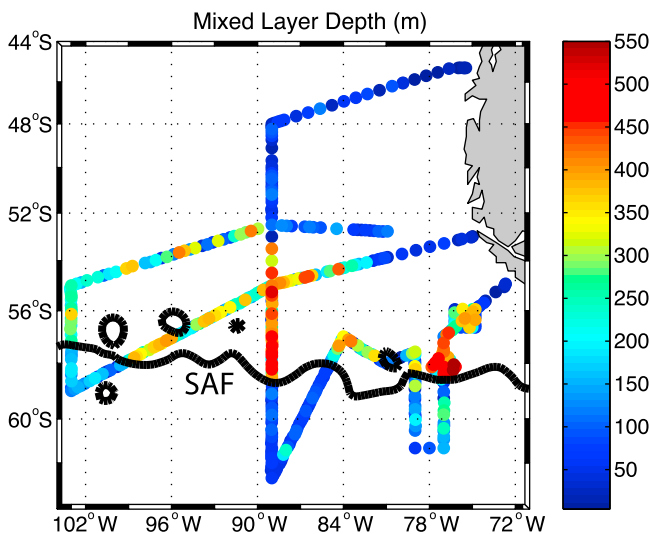

Figure 2. Mixed layer depth at CTD and XCTD stations for the 2005 austral winter cruise extend from 0 m (blue) to 550 m (red). The mean AVISO dynamic topography contour that most closely matched the SAF location in hydrography and ADCP data is also plotted (black line). The mean dynamic topography was calculated over the cruise period, August 23 to October 5, 2005. The three sections plotted in Figure 3 were taken along 103°W, 89°W and 77°W.

[14] The 135 CTD/rosette stations from the 2005 austral winter cruise and 105 stations from the 2006 austral summer cruise provided full depth profiles of potential temperature (referred to as temperature throughout the remainder of the paper), salinity, and oxygen in the SAMW and AAIW formation region. Bottle samples (from a 24 bottle rosette in winter and a 36 bottle rosette in summer) were analyzed for dissolved oxygen, salinity, and nutrients. These data were acquired and processed by Scripps Institution of Oceanography's Ocean Data Facility. Carbon parameters and chlorofluorocarbons were also collected during the winter cruise [*Hartin et al.*, 2011].

[15] Intensive XCTD sampling complemented the CTD stations by providing higher vertical and horizontal resolution observations of the mixed layer and frontal and eddy structure, but profiled to only 1100 meters. 371 XCTDs were deployed during the 2005 austral winter cruise and 352 were deployed during the 2006 austral summer cruise. Generally, three XCTDs were deployed by hand launcher from the rear of the ship between CTD stations, resulting in typical XCTD spacing of 15 km. The XCTDs were TSK probes from Sippican. Many XCTDs failed during the 2005 austral winter cruise because of a grounding problem with the ship's data acquisition computer. Scripps Institution of Oceanography provided a data acquisition computer for the 2006 austral summer cruise, and XCTD failure rates were greatly reduced.

[16] A quality control process following *Albérola et al.* [1996] was implemented to offset XCTD profiles that deviated greatly from neighboring CTD profiles. This method uses a linear regression in θ-salinity space to calculate salinity offsets for XCTDs. It presumes that neighboring CTD and XCTD profiles should have the same θ-salinity relationship at depth; this is not always the case in highly variable frontal regions. Applying the method reduced XCTD salinity variance at depth. XCTDs that greatly differed from nearby CTD stations were discarded. Due to the response of the conductivity sensor, many profiles exhibit spurious salinity values near the surface, usually in the form of unrealistically high salinity tails that gradually blend into

the mixed layer. These profiles were trimmed as deeply as necessary to remove the spurious data. Only profiles deeper than 400 m were used in this study. These quality controls reduced the number of available profiles to 303 for the 2005 austral winter cruise and 342 for the 2006 austral summer cruise. To eliminate high frequency noise in the XCTD salinity profiles, the XCTD temperature and salinity profiles were smoothed with a 5 m running-mean filter.

[17] The underway and lowered acoustic Doppler current profiler data sets (SADCP and LADCP, respectively) are described by *Chereskin et al.* [2010]. The SADCP unit, a RD Instruments 75 kHz Ocean Surveyor, was averaged into 10 m depth bins centered from 50 m to 810 m. The SADCP data was binned into 5 minute average profiles. The LADCP, a 150 kHz RD Instruments Phase 3 broadband ADCP, sampled full depth profiles from 60 m interpolated to a 20 m sampling interval.

[18] Both cruises collected underway temperature, salinity, and dissolved oxygen data, providing a record of the surface layer at very high resolution. Similarly, the Improved Meteorological (IMET) sensors mounted on R/V *Knorr* measured air temperature, wind strength and direction, sea level pressure, shortwave radiation, humidity, and precipitation; there was no longwave radiation sensor. The underway and IMET data were reported at 30 second intervals. The COARE bulk algorithm [*Fairall et al.*, 2003] was applied to the raw IMET and underway temperature data to produce latent and sensible heat fluxes. These instantaneous fluxes were averaged into one-hour bins. The widely-used National Centers for Environmental Prediction (NCEP) Reanalysis-1 [*Kalnay et al.*, 1996] longwave fluxes were linearly interpolated to the one-hour bins to calculate net heat fluxes. Incorporating longwave fluxes from another commonly-used reanalysis product from the European Center for Medium range Weather Forecasting (ECMWF) did not alter the findings.

[19] Thirteen Argo floats were deployed during the 2005 winter cruise. Argo has continuously sampled the cruise region since 2003, providing greater temporal coverage but reduced horizontal and vertical resolution relative to the cruise. The mixed layer depths and properties from 8703 Argo profiles collected in the cruise region between January 2003 and February 2010 were calculated using the algorithm developed by *Holte and Talley* [2009]. Argo data are available online (Table 1).

[20] Remote sensing observations are used to identify the large-scale conditions in the SAMW formation region. QuikSCAT winds provide the overall wind field and show the passage of storms. AMSR-E supplies microwave sea surface temperature (SST) observations. QuikSCAT and AMSR-E provide daily fields with 0.25 degree resolution. AVISO merged satellite topography, available weekly on a 0.25 degree grid, is used to identify eddies, map the geostrophic flow, and determine the relationship of the SAMW mixed layers to the SAF. These products are all available online (Table 1).

3. Mixed Layer Observations

[21] Observations from the 2005 austral winter cruise reveal a band of deep mixed layers extending north from the SAF (Figure 2). The cruise mixed layer depths were identified through individual inspection. Forty-two profiles with mixed layers deeper than 400 m were observed. The latitudinal extent of the band of deep mixed layers decreases eastward; along 89°W the band's latitudinal extent is 6°, whereas just upstream of Drake Passage the latitudinal extent is 3°. The deepest mixed layers, to 550 m, are found just upstream of Drake Passage. Along the western section at 103°W the MLDs are between 200 and 300 m. The SAMW mixed layers are influenced by the meanders and eddies of the SAF, which forms the southern boundary of the SAMW formation region. The cruise track crossed two cold core eddies in the SAMW formation region at approximately 96°W and 57°S and 80°W and 58°S. These eddies modulated the MLD, decreasing it by more than 200 m compared to the nearby SAMW mixed layers (Figure 2). South of the SAF, profiles are characterized by interleaving temperature-salinity layers and decreased mixed layer temperature, salinity, and depth relative to the deep SAMW mixed layers north of the SAF (Figures 2 and 3). Within this region south of the SAF, several locally-unusual deep mixed layers of nearly 300 m were observed along 77°W. At the SAMW formation region's northern boundary, the SAMW was capped by shallower, fresher, and warmer mixed layers.

[22] The vertical and horizontal structure of the SAMW mixed layers in austral winter 2005 is evident from sections at 103°W, 89°W, and 77°W (Figure 3). The SAMW is identifiable in each section as a large, uniform mass of water extending north from the SAF. In all sections the deepest SAMW mixed layers occurred immediately north of the SAF, usually within 100 km of the front. In the westernmost section at 103°W, the SAMW had a density range of 26.95 to 27.0 kg m^{-3}. Along 89°W the SAMW had potential densities between 27.0 and 27.02 kg m^{-3}. At the section closest to Drake Passage, along 77°W, the SAMW had potential densities between 27.02 and 27.04 kg m^{-3}. The SAMW in each section was not completely uniform. Along 89°W, the SAMW within 2° of the SAF was approximately 0.4°C colder and 0.05 psu fresher than the SAMW farther north along the same section (Figure 3); it also had a lower oxygen fractional saturation of 96%. This suggests that the mixed layer recently overturned and entrained the lower-oxygen waters beneath the mixed layer, as also noted by *Hartin et al.* [2011].

[23] The SAMW mixed layers are characterized by higher salinities relative to neighboring waters (Figure 4). The deep SAMW mixed layers form a cluster in temperature-salinity space and have salinities ranging from approximately 34.075 to 34.2 psu. Outside of the cluster of deep SAMW mixed layers, the mixed layers have lower salinities between approximately 33.95 and 34.075 psu. This pattern appears to persist throughout the year; the highest salinities observed during the 2006 austral summer cruise were found in the SAMW formation region (not shown). *Ren et al.* [2011] suggest that mixed layer entrainment is important in maintaining the higher salinities of the SAMW band.

[24] The cluster of SAMW is organized spatially into two groups (Figure 4). One group is composed of mixed layers from the western portion of the cruise with potential densities less than 27.0 kg m^{-3}; the other is composed of mixed layers from the cruise's eastern sections upstream of Drake Passage with potential densities greater than 27.0 kg m^{-3}. In terms of potential density, these spatial groups correspond to an along-front variation in mixed layer potential density

Table 1. Online Data Sources[a]

Data Source	Spatial Resolution	Temporal Resolution	Web Site
Argo	NA	NA	http://www.usgodae.org/argo/argo.html
AMSR-E	0.25°	24 hr	http://www.ssmi.com/sst/microwave_oi_sst_browse.html
QuikSCAT	0.25°	24 hr	http://podaac.jpl.nasa.gov/quikscat/
AVISO	0.25°	168 hr	http://www.aviso.oceanobs.com/index.php?id=1272
NCEP	1.875°	6 hr	http://www.esrl.noaa.gov/psd/data/reanalysis/reanalysis.shtml
ECMWF	1.5°	12 hr	http://data-portal.ecmwf.int/data/d/interim_daily/
J-OFURO	1°	24 hr	http://dtsv.scc.u-tokai.ac.jp/j-ofuro/
OAFlux	1°	24 hr	http://oaflux.whoi.edu/data.html

[a]NA, not available.

of 0.05 kg m^{-3} over a distance of 1500 km. In Argo, this downstream change in SAMW potential density is continuous; the distinct grouping is the result of the cruise spatial sampling.

4. Air-Sea Forcing: Cruise Observations

[25] In this study, we evaluate the extent to which SAMW formation can be considered a one-dimensional mixed layer process driven by local air-sea buoyancy fluxes and wind mixing. By focusing on one aspect of SAMW formation we are able to examine a number of forcing scenarios. Holte et al. (manuscript in preparation, 2012) study the influence of cross-frontal exchange on SAMW formation.

[26] The buoyancy flux has two components, a thermal component due to heat fluxes and a saline component due to
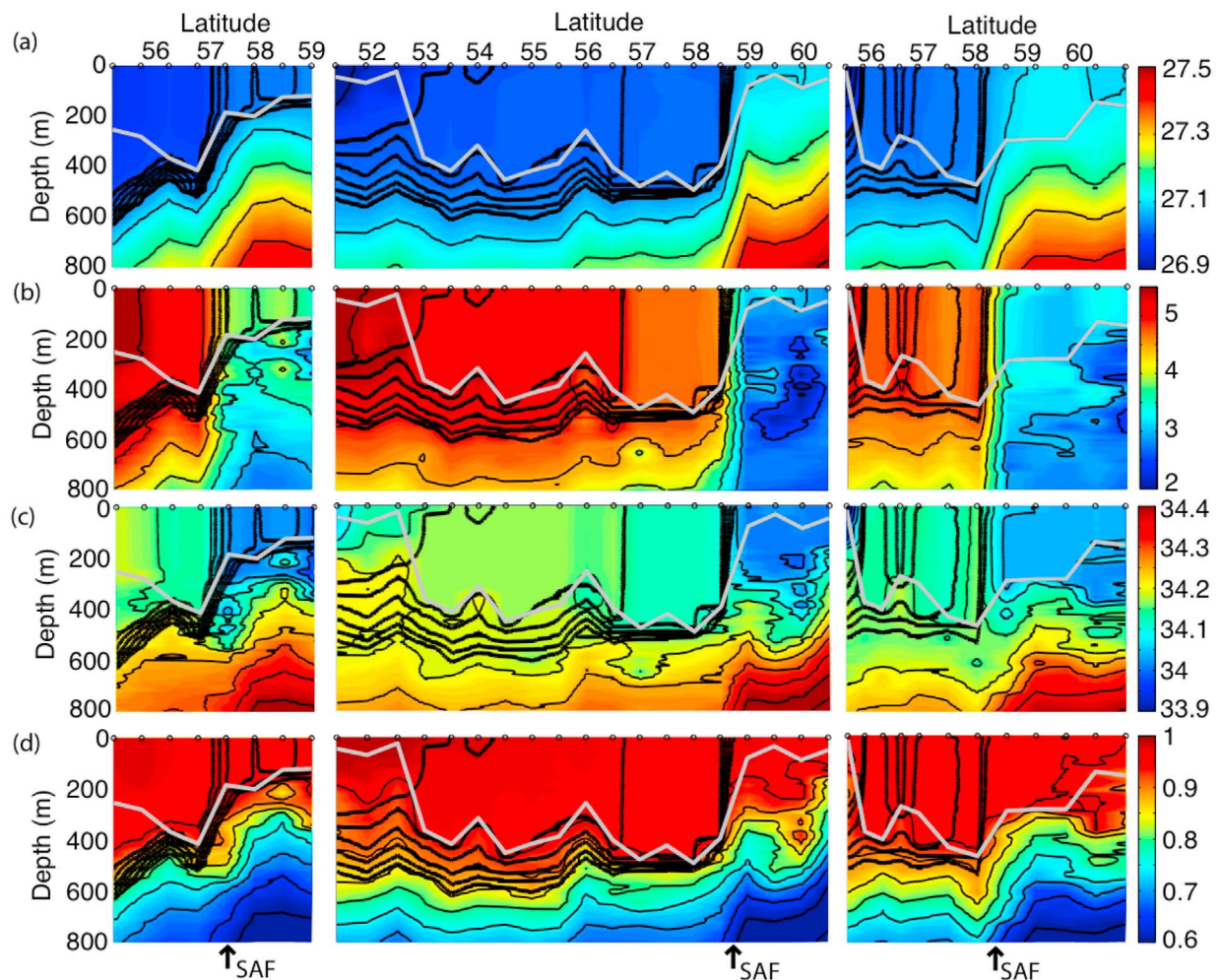

Figure 3. Sections of (a) potential density (kg m^{-3}), (b) potential temperature (°C), (c) salinity (psu), and (d) oxygen fractional saturation along (left) 103°W, (middle) 89°W, and (right) 77°W from the 2005 austral winter cruise (south on the right). The CTD profile locations are denoted by circles at the surface. The 27, 27.01, 27.02, 27.03, 27.04, and 27.05 kg m^{-3} isopycnals are contoured by bold black lines. The grey line is the mixed layer depth. For each section, the location of the SAF is identified by a rapid shallowing of isopycnals and is marked by arrows.
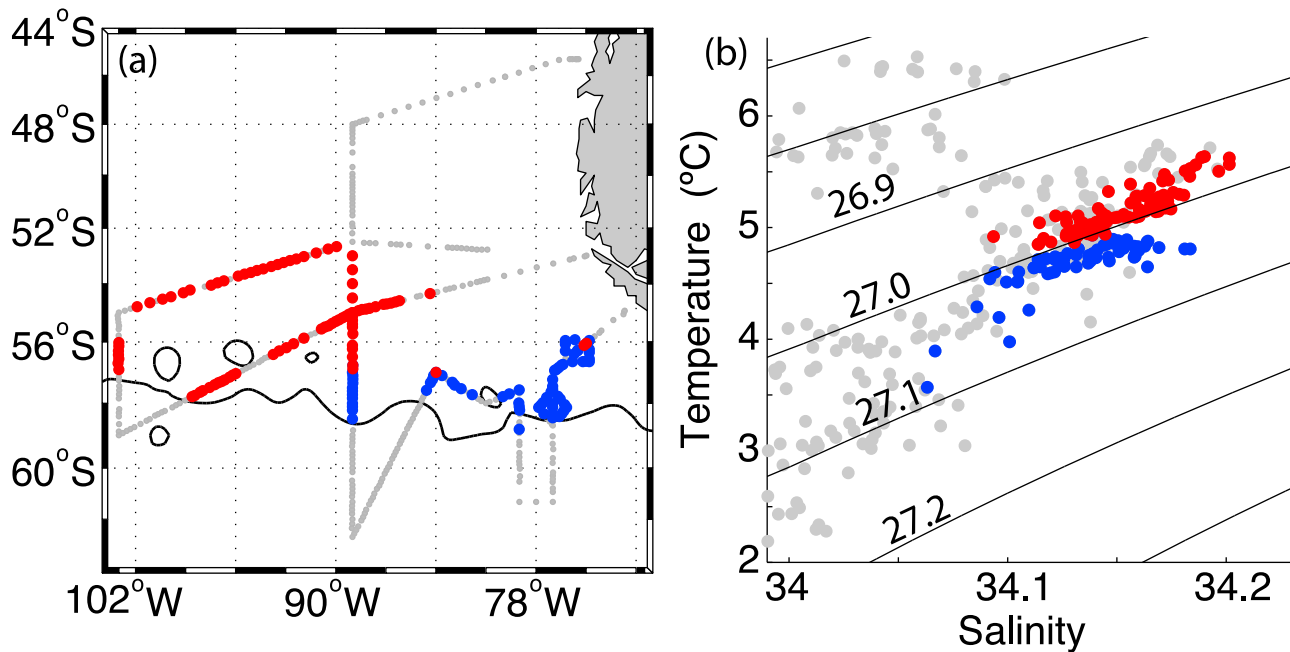
Figure 4. The (a) geographical distribution and (b) temperature-salinity diagram of mixed layers deeper than 200 m from the 2005 austral winter cruise, using all CTD and XCTD profiles. Mixed layers with densities greater than 27.0 kg m^{-3} are plotted in blue; those with densities less than 27.0 kg m^{-3} are plotted in red. Grey dots denote the remainder of the CTD and XCTD profiles. In Figure 4a, the mean AVISO dynamic topography contour that most closely matched the SAF location in hydrography and ADCP data is plotted (black line). Potential density (black lines) is contoured in Figure 4b at 0.1 kg m^{-3} intervals.

evaporation and precipitation. The equation for the buoyancy flux is

$$B = \frac{g\alpha}{c_p}(Q_{sh} + Q_{lh} + Q_{lw} + Q_{sw}) + gS\beta(P - E), \quad (1)$$

where $\alpha = \rho^{-1} \, \partial\rho/\partial T$ and $\beta = \rho^{-1} \, \partial\rho/\partial S$ are the thermal and saline expansion coefficients of seawater (which depend on the surface temperature and salinity, T and S), c_p is the specific heat capacity of water, g is the acceleration due to gravity, Q_{sh} is the sensible heat flux, Q_{lh} is the latent heat flux, Q_{lw} is the net longwave radiation, and Q_{sw} is the incoming solar radiation at the sea surface. These heat flux terms determine the thermal component of the air-sea buoyancy flux. During winter, ocean heat loss to the atmosphere, in the form of latent, sensible, and longwave heat fluxes, destabilizes the water column; the surface density increases, resulting in convective overturning. Shortwave heat fluxes stabilize the surface layer. The freshwater buoyancy component depends on the surface salinity and the difference between precipitation, P, and evaporation, E. Evaporation is calculated as $E = Q_{lh}/L_v$, where L_v is the latent heat of vaporization [*Sathiyamoorthy and Moore*, 2002]. Evaporation increases the surface density, whereas precipitation freshens the surface water, decreasing the density and stabilizing the surface layer. We use the convention that a negative heat flux corresponds to ocean heat and buoyancy loss.

[27] During the 2005 austral winter cruise the regions of oceanic heat loss generally corresponded to regions with deep SAMW mixed layers (Figures 2, 5, and 6). The correlation between the MLD and the heat flux was −0.44. The largest winter heat losses, nearly −200 W m^{-2}, were observed along 77°W. These are small compared to the fluxes of nearly −1000 W m^{-2} that are associated with the formation of Subtropical Mode Waters near the Gulf Stream and Kuroshio [*Joyce et al.*, 2009]. Large fluxes exceeding −100 W m^{-2} were also observed north of the SAF along 89°W and between 96°W and 83°W. The large heat fluxes, and their correspondence to the deep mixed layers, suggest that active mixing occurred during the survey [*Sloyan et al.*, 2010]. In the northern and northwestern sectors of the cruise the heat flux is small, and at times positive; deep SAMW mixed layers were observed sporadically in these regions.

[28] The largest heat fluxes observed during the winter cruise were caused by winds from the south; the correlation between the sum of the sensible and latent heat fluxes and the northward wind velocity was −0.55. The winds recorded during the 2005 cruise exhibited considerable variation in direction and magnitude (Figure 7), reflecting the many synoptic storms that passed through the SAMW formation region during the cruise; the predominant wind directions are southwesterly and northwesterly. The SAMW formation region is remote from any upstream continental land masses that could produce extreme cold air outbreaks, so the cold polar waters south of the SAF serve as the largest atmospheric heat sink in the region. Winds from the south originate over this relatively cold region, and when they blow north across the SAF, they encounter warmer water. This creates the air-sea temperature difference that produces large
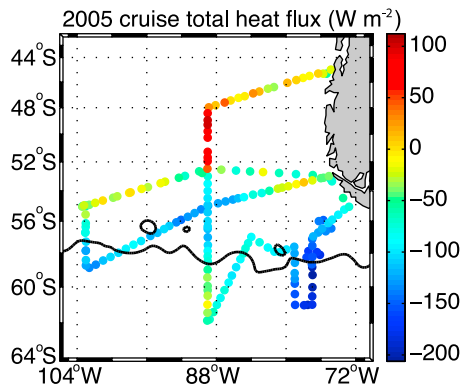
Figure 5. Total synoptic heat fluxes along the 2005 cruise track ranged from 100 W m^{-2} (red, ocean heat gain) to −200 W m^{-2} (blue, ocean heat loss). The instantaneous latent and sensible heat fluxes were calculated using the COARE algorithm from cruise IMET data. Shortwave fluxes were measured by the IMET system. Longwave fluxes are from NCEP reanalysis. The fluxes are six-hour averages smoothed with a 2 day running mean to soften daily peaks in the shortwave radiation and plotted every six hours. The mean AVISO dynamic topography contour that most closely matched the SAF location in hydrography and ADCP data is also plotted (black line).

sensible and latent heat fluxes over the SAMW formation region (Figure 7).

[29] These heat fluxes contributed to active mixing in the SAMW formation region. The deepest mixed layers tended to have fractional oxygen saturations of 0.96 and corresponded to the largest synoptic heat fluxes at the surface (Figure 6). These low fractional oxygen saturations are typical signatures of active mixed layer deepening; as the mixed layer deepens it entrains water at its base that has a lower oxygen fractional saturation, lowering the fractional oxygen saturation of the entire mixed layer. Similarly, an undersaturated chlorofluorocarbon (CFC) content was observed in the deep mixed layers on the 2005 austral winter cruise for the same reason [*Hartin et al.*, 2011]. The mild oxygen and CFC depletion of about 4% contrasts with the larger undersaturation, about 10%, of deep convection regions [*Talley et al.*, 2003]; this suggests that SAMW forms by gradual winter deepening rather than episodic deep convective penetration. The mixed layers with the most vertically uniform oxygen saturations were located immediately near the SAF (Figure 3). Away from the front the mixed layer fractional oxygen saturation has a slight vertical gradient, increasing toward the surface. The oxygen distributions suggest that the mixing was most active near the front.

5. Air-Sea Forcing: Observations and Flux Products Comparison

[30] The cruise IMET heat fluxes described in section 2 are compared to various reanalysis and observation-derived heat flux products. We use fields from NCEP Reanalysis 1 [*Kalnay et al.*, 1996], ECMWF Interim, Japanese Ocean Flux Data sets with Use of Remote Sensing Observations (J-OFURO), Kelly, OAFlux, and the Southern Ocean State Estimate (SOSE). The heat flux products provided by

NCEP, ECMWF, J-OFURO, and OAFlux are available online (Table 1). The reanalysis products, NCEP and ECMWF, provide flux fields four times and two times daily, respectively; the other products are available once daily. J-OFURO, Kelly, and OAFlux are mostly derived from direct observations. J-OFURO primarily incorporates remote sensing data. The Kelly latent and sensible heat fluxes are computed by Kathryn A. Kelly's group at the University of Washington with the COARE v3.0 algorithm, using QuikSCAT wind speed maps, the NOAA OISST sea surface temperature product (http://www.ncdc.noaa.gov/oa/climate/research/sst/oi-daily.php), and ECMWF analyses for the remainder of the input variables. Kelly fluxes have 0.5° resolution. OAFluxes are derived from satellite observations, surface observations, and reanalyzed atmospheric models [*Yu et al.*, 2008]. SOSE synthesizes NCEP fluxes and a wide variety of observations in an eddy-permitting model; it outputs, among many other fields, modified NCEP fluxes that are consistent with the in situ observations [*Mazloff et al.*, 2010]. Products missing any of the four heat flux terms, wind stress, or precipitation are supplemented with the NCEP fields (Table 2).

[31] In general, most of the products' along-track total heat fluxes compare to the total heat fluxes observed during the 2005 and 2006 cruises fairly well, capturing the high and low heat flux events from both cruises (Figure 8) [comparison for the 2006 cruise not shown]. NCEP, ECMWF, and Kelly fluxes most closely match the cruise fluxes, particularly for the 2005 austral winter cruise. *Cerovecki et al.* [2011], in an evaluation of NCEP and ECMWF fluxes in the Southern Ocean, found that the products' net heat fluxes were extremely similar in the southeast Pacific over the period 2005–2007 [*Cerovecki et al.*, 2011, Figure 2b]. All of the heat flux products deviate more from the 2006 austral summer cruise fluxes than they do from the 2005 austral winter cruise fluxes (Table 3). J-OFURO and SOSE have the poorest fits to the cruise observations and produce many spurious heat flux events, though SOSE's mean fluxes are similar to the cruise mean. J-OFURO has the largest root
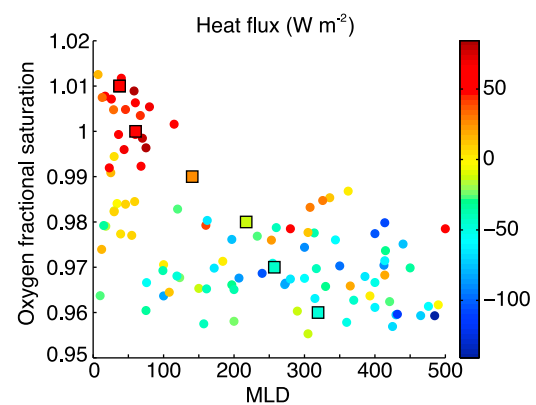

Figure 6. Comparison of mixed layer oxygen saturation and MLD for CTD profiles north of the SAF (colored circles). The color corresponds to total synoptic heat flux. The mean heat flux and mean mixed layer depth are calculated for mixed layer oxygen saturation bins centered at 0.96, 0.97, 0.98, 0.99, 1, and 1.01 (colored squares).
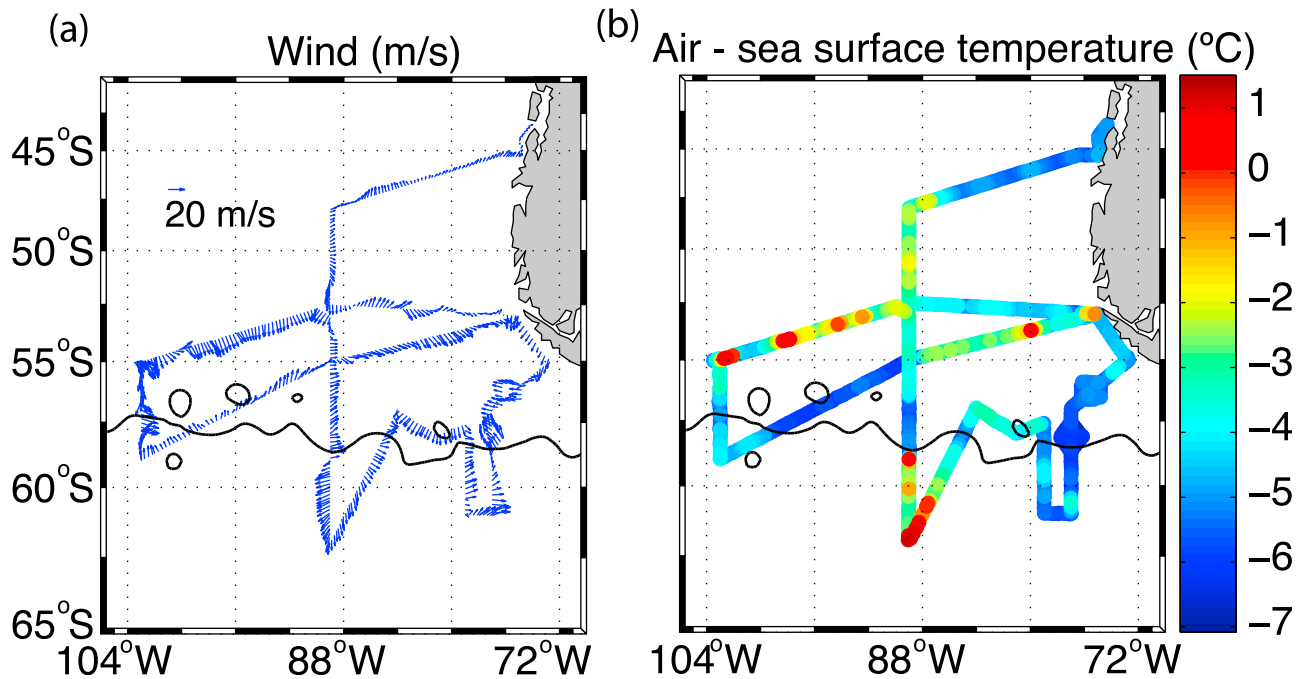
Figure 7. Maps of (a) vector wind (m/s) and (b) air-sea temperature difference (°C) along the 2005 cruise track. The mean AVISO dynamic topography contour that most closely matched the SAF location in hydrography and ADCP data is also plotted (black line).

mean square differences from the cruise fluxes. OAFlux is biased more than 30 W m^{-2} higher (less ocean heat loss) than the cruise fluxes.

[32] The latent and sensible heat fluxes have roughly the same magnitudes as each other (Figure 8). Surprisingly, the sum of the latent and sensible heat fluxes is the same for both the austral winter and summer cruises (Table 3). The northward wind mechanism that produces the enhanced ocean heat fluxes during the winter cruise (Figure 7) also works in summer, even though the temperature gradient across the SAF is reduced in summer. During summer the shortwave heat flux overwhelms the latent and sensible heat fluxes, so the net heat flux is positive.

[33] Besides heat fluxes, air-sea fluxes of momentum and precipitation are also important to SAMW formation. NCEP and QuikSCAT closely track the wind measurements from the 2005 winter cruise (Figure 9). NCEP captures the large synoptic storms, on the scale of 5 days, and also shorter scale fluctuations. In the one-dimensional model runs, NCEP wind stress is used as the default wind stress for the flux products that do not provide wind fields (e.g. Kelly and OAFlux). Accurate precipitation measurements are difficult to obtain at sea, especially in high-wind conditions [*Yuter*

and Parker, 2001]. ECMWF and NCEP are the only products that provide precipitation.

6. One-Dimensional Mixed Layer Modeling With Observed Forcing

[34] A one-dimensional KPP mixed layer model [*Large et al.*, 1994] is used to assess the role of buoyancy forcing and wind mixing in forming deep winter SAMW mixed layers from stratified summer profiles. Five sets of runs are evolved in the model, each with different sources for the heat, precipitation, and momentum fluxes; the NCEP, ECMWF, Kelly, J-OFURO, and OAFlux forcing fields used in each set of runs are outlined in Table 2. Each set of the five model runs is initialized with 100 CTD profiles from the 2006 austral summer cruise. The fluxes are interpolated to each profile location, commence on each profile's collection date, and evolve the profiles for one year. To allow comparison with the 2005 cruise observations and with winter Argo profiles collected in the cruise region, a representative simulated winter mixed layer is calculated at each CTD station as the temporal mean of each model run during the month of August, producing 100 simulated winter mixed

Table 2. Forcing Fields Provided for Each Flux Product[a]

Product	Latent	Sensible	Longwave	Shortwave	Momentum	Precipitation
NCEP	NCEP	NCEP	NCEP	NCEP	NCEP	NCEP
ECMWF	ECMWF	ECMWF	ECMWF	ECMWF	ECMWF	ECMWF
Kelly	Kelly	Kelly	NCEP	NCEP	NCEP	NCEP
J-OFURO	J-OFURO	J-OFURO	J-OFURO	J-OFURO	J-OFURO	NCEP
OAFlux	OAFlux	OAFlux	OAFlux	OAFlux	NCEP	NCEP

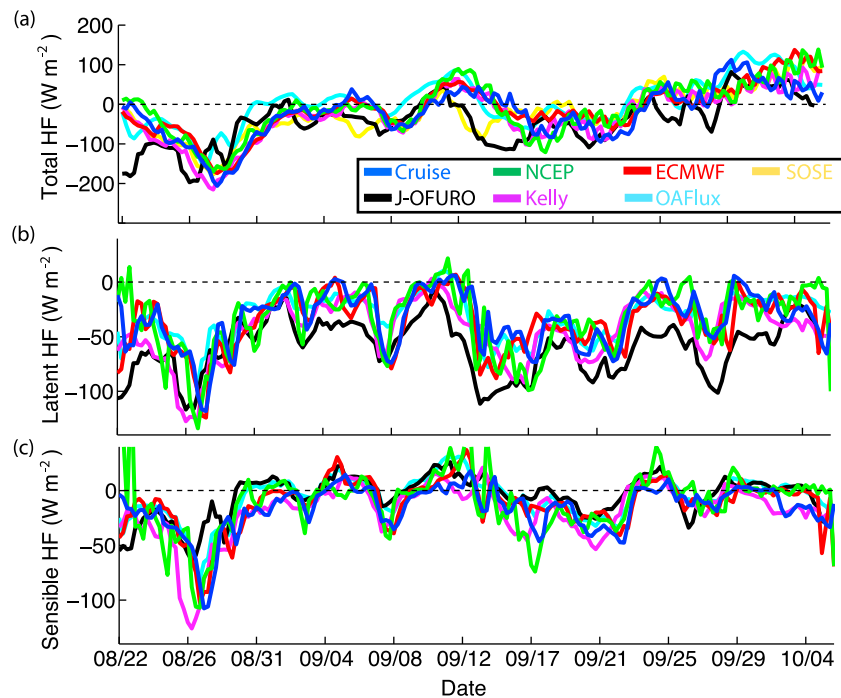[a]NCEP is used as the default for any missing forcing terms.

Figure 8. Along track values of synoptic (a) total heat flux, (b) sensible heat flux, and (c) latent heat flux for the 2005 winter cruise for: cruise IMET fluxes (blue), NCEP reanalysis (green), ECMWF (red), SOSE (yellow), OAFluxes (cyan), Kelly fluxes (magenta), and J-OFURO (black). The cruise IMET latent and sensible heat fluxes are calculated with the COARE algorithm. The cruise total heat flux uses measured IMET shortwave fluxes and NCEP reanalysis for longwave fluxes. The cruise fluxes are six-hour averages smoothed with a 2 day running mean. The flux products are also smoothed with a 2 day running mean. The dashed line in each plot marks the zero level.

layers for each flux product. August was chosen for calculating the mean because the maximum mean Argo MLD occurs in August and the heat flux becomes positive after August. Averaging the simulations over longer winter periods does not substantially alter the results.

[35] We use a simple configuration of the Regional Ocean Modeling System (ROMS) for our one-dimensional KPP mixed layer model (available at: http://www.myroms.org/). We run ROMS in its typical 3-D configuration, utilizing a 10 by 10 horizontal grid with periodic boundaries, and repeat the initial profile and forcing at every grid point, giving us in essence a 1-D configuration. The model is initialized with 250 depth levels and a profile depth of 2000 m, producing a grid with an average spacing of 5 m in the upper 500 m. The profiles are evolved for one year with a time step of 60 seconds; the fluxes are interpolated to match this time step. ROMS has many possible configurations. We tested 20 different configurations, using different combinations of the KPP mixing scheme of *Large et al.* [1994], the *Kantha and Clayson* [1994] stability function, and the *Mellor and Yamada* [1982] level 2.5 closure scheme, as well as various numerical modules in ROMS, such as the tracer advection schemes. To test the model set-up, each configuration was run for three different initial CTD profiles

Table 3. Means and Root-Mean-Square Differences of Along Track Total Heat Flux and Sensible and Latent Heat Fluxes From the Two Cruises Compared to the Various Flux Products[a]

	Cruise	NCEP	ECMWF	SOSE	Kelly	J-OFURO	OAFlux
			Mean				
2005 total heat flux	−41	−33	−33	−43	−47	−56	−13
2005 latent + sensible	−52	−52	−51	NA	−65	−63	−40
2006 total heat flux	40	63	61	45	69	51	81
2006 latent + sensible	−51	−47	−43	NA	−39	−40	−31
			Root-Mean-Square Differences				
2005 total heat flux		30	19	43	27	53	38
2005 latent + sensible		36	20	NA	38	33	24
2006 total heat flux		48	39	46	43	68	43
2006 latent + sensible		46	37	NA	35	36	30

[a]The flux products are interpolated to the cruise locations and times. All of the fluxes are smoothed with a 2 day running mean. The root-mean-square differences are calculated as the difference between the cruise heat flux and the various products' heat fluxes. NA, not available.
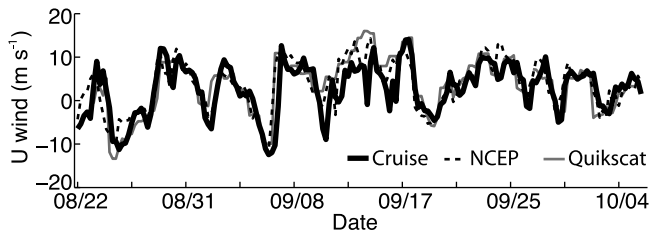
Figure 9. Along track wind from the 2005 cruise (black line) compared to NCEP (dashed line) and QuikSCAT (grey line) winds.

from the 2006 austral summer cruise: two in the SAMW formation region (station 143 at 76°W and 56.5°S and station 147 at 77°W and 58°S) and one south of the SAF (station 154 at 77°W and 61.5°S). The three profiles were evolved for one year with NCEP forcing corresponding to the CTD locations. Most of the 20 configurations produced remarkably similar winter SAMW mixed layer depths and properties; for each initial profile the configurations' maximum winter MLDs differ by less than 80 m. The chosen configuration is essentially the KPP mixed layer model, which includes diffusive mixing due to shear instability, convective mixing due to shear instability, double-diffusive mixing, with non-local transport activated. Our set-up differs slightly from the standard configuration; we use splines

vertical advection because of the high vertical resolution of our simulation. We also conducted test runs with the Price-Weller-Pinkel mixed layer model [*Price et al.*, 1986] and NCEP forcing, but its simulated SAMW mixed layers were unrealistically shallow.

[36] In terms of MLD, the five forcing products all produce some sort of SAMW, in that they all produce deep mixed layers in the region where SAMW was observed during the 2005 austral winter cruise (Figure 10). They all correctly reproduce the band of deep SAMW mixed layers north of the SAF. The band of MLDs is wider to the west, and the mixed layers generally deepen to the east. This mirrors the 2005 austral winter cruise MLDs and the range of Argo MLDs. Argo is useful for comparison because its profiles span several winters, from 2003 to 2009, and are scattered throughout the SAMW formation region, providing greater spatial- and temporal-coverage than any ship-based observations. In the Argo data, the band of deep winter SAMW mixed layers narrows near Drake Passage and has largely the same areal extent as the SAMW observed during the 2005 austral winter cruise. Argo features more numerous and deeper SAMW mixed layers in the cruise's western section. Argo recorded 10 MLDs deeper than 600 m, whereas the deepest MLDS observed during the 2005 austral winter cruise reached 550 m. All of the forcing products except for OAFlux tend to produce deeper SAMW MLDs than were observed during the cruise. NCEP and
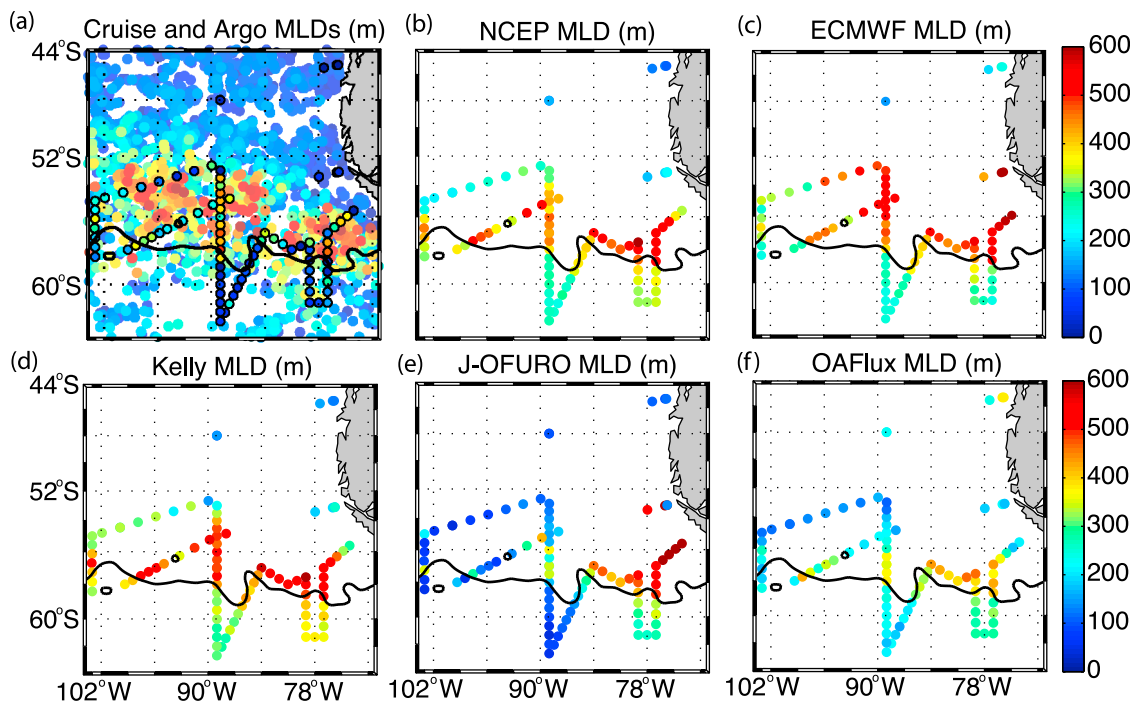

Figure 10. MLDs from (a) Argo and (b–f) simulated winter MLDs from KPP runs initialized with 2006 summer cruise profiles. The simulated runs are forced with NCEP (Figure 10b), ECMWF (Figure 10c), Kelly (Figure 10d), J-OFURO (Figure 10e), and OAFluxes (Figure 10f). The MLDs range from 0 meters (blue) to 600 meters (red). In Figure 10a, the cruise CTD MLDs are plotted as colored circles with black borders. 2597 winter Argo profiles (collected between July and October from 2003 to 2010) are plotted as colored circles with no borders. The mean AVISO dynamic topography contour that most closely matched the SAF location in hydrography and ADCP data during the 2006 cruise is also plotted (black line). The mean dynamic topography was calculated over the 2006 cruise period.
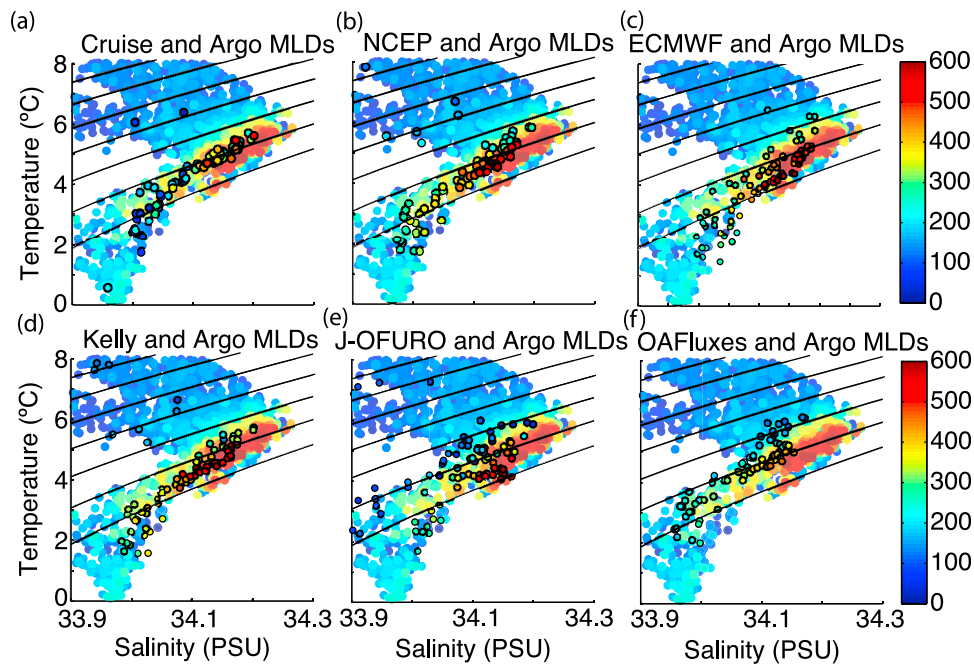
Figure 11. Temperature-salinity diagrams from (a) 2005 cruise and (b–f) simulated winter MLDs from KPP runs initialized with 2006 summer cruise profiles. The simulated runs are forced with NCEP (Figure 11b), ECMWF (Figure 11c), Kelly (Figure 11d), J-OFURO (Figure 11e), and OAFluxes (Figure 11f). The cruise and simulated mixed layers are plotted in colored circles with black borders. The mixed layers from 2597 winter Argo profiles (collected between July and October from 2003 to 2010) in the cruise region are plotted as colored circles without borders. The MLDs range from 0 meters (blue) to 600 meters (red). The potential density is contoured at 0.1 kg m^{-3} intervals from 26.5 to 27.1 kg m^{-3}.

Kelly produce very similar MLDs to each other because the Kelly model runs use NCEP longwave, shortwave, precipitation, and wind stress fields (Table 2).

[37] The observed and simulated SAMW mixed layers differ in a number of ways. To compare the simulated SAMW mixed layers to observations, for each CTD station we calculate the average of the two deepest Argo mixed layers collected within 100 km of the station; the root mean square difference between the simulated mixed layers and the Argo field is then calculated for MLD, temperature, and salinity. NCEP, Kelly, and ECMWF fluxes produce the fields with the smallest MLD root mean square differences, 95, 79, and 89 m, respectively. The next smallest root mean square difference is 195 m. J-OFURO and OAFlux produce few deep SAMW MLDs in the cruise's western sections. OAFlux produces shallower MLDs throughout the SAMW formation region; it only produces MLDs to depths of approximately 400 m in a very thin band just north of the SAF. J-OFURO, and OAFlux produce more accurate MLDs south of the SAF, whereas NCEP, ECMWF, and Kelly's MLDs south of the SAF are more than 100 m deeper than the MLDs observed on the 2005 austral winter cruise. Argo has recorded MLDs to 350 m south of the SAF, so the MLDs produced by these fluxes are possible.

[38] The temperature-salinity characteristics of the simulated SAMW mixed layers generally match the Argo observations (Figure 11). The NCEP, ECMWF, and Kelly mixed layers overlap the Argo SAMW more than the J-OFURO and OAFlux mixed layers; NCEP and Kelly fluxes produce the smallest root mean square differences for temperature and salinity. The SAMW mixed layers produced by OAFlux are too fresh, with no simulated SAMW mixed layer salinities greater than 34.15 psu. None of the simulated SAMWs capture the full range of the Argo SAMW salinities, and in general they tend to reproduce the fresher SAMWs in the cruise region. Similarly, the cruise SAMW mixed layers do not have as wide a range of salinities as the Argo SAMW mixed layers.

[39] Figure 12 shows a time series of simulated MLDs and forcing fields for three regions from the cruise. The simulated MLDs generally fall within the range of Argo observations. The deepest Argo SAMW MLDs occur in August, whereas the model runs have much longer periods of deep MLDs. This discrepancy suggests that lateral processes are important to restratification. The deepening in the simulated eastern profiles seems to correspond to a peak in the wind stress forcing in May. By the end of winter the cumulative forcing fluxes for the three groups of profiles are largely the same.

[40] Examining the mean forcing fields for the period from February to September, 2006, illuminates some of these differences in the simulated SAMW mixed layers. This period runs approximately from each profile's collection date during the 2006 austral summer cruise to the following winter. NCEP, ECMWF, Kelly, and J-OFURO mean heat flux fields are quite similar in the SAMW formation region. The NCEP and ECMWF fluxes in Figure 12a are representative of these fields. There is little zonal variation in heat
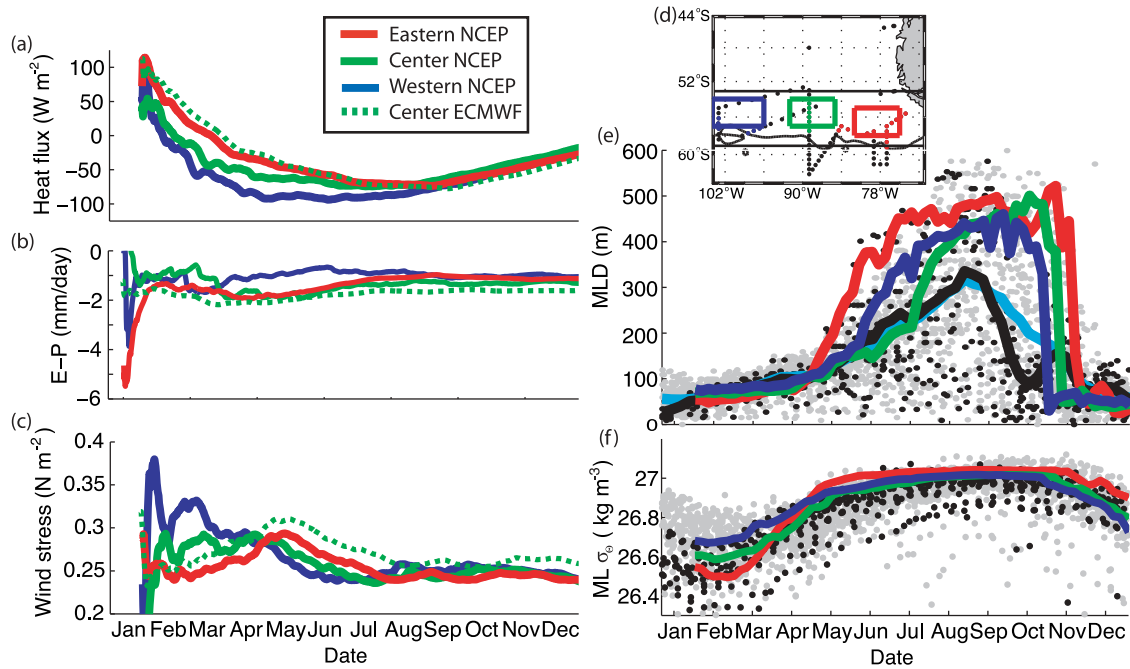
Figure 12. Spatial-mean cumulative (a) heat flux, (b) evaporation minus precipitation, (c) wind stress, and mean (e) MLD and (f) mixed layer potential density. The mean cumulative air-sea fluxes in Figures 12a–12c were calculated from 2006 NCEP fields (colored lines, corresponding to colored boxes in Figures 12d) and 2006 ECMWF fields (dashed green line, corresponding to green box in Figure 12d). (d) The CTD stations (dots) sampled on both cruises are plotted; the highlighted groups of blue, green, and red CTD stations are used to calculate the mean mixed layer properties in Figures 12e and 12f. The mean AVISO dynamic topography contour that most closely matched the SAF location in hydrography and ADCP data is also plotted (black line). In Figures 12e and 12f, the mean simulated mixed layer depths and potential densities for the groups of CTD stations are plotted, as well as the Argo values (grey dots) for all profiles collected within the black box in Figure 12d. The black dots denote Argo from 2006. In Figure 12e, the mean Argo MLD for all years is the cyan line; the mean Argo MLD for 2006 is the black line.

flux in both NCEP and ECMWF, though the fluxes are slightly stronger in the cruise's southeast section, where the deeper MLDs were simulated. J-OFURO features a stronger zonal gradient, with the strongest negative fluxes closer to Chile; these strong fluxes produce unrealistically deep MLDs near Chile (Figure 10e). The shallower MLDs produced in the northwestern cruise sections by all of the flux products are due to lower heat loss in these sections. OAFlux produces shallower SAMW MLDs throughout the SAMW formation region because its mean February to September heat fluxes are more than 10 W m^{-2} less negative than the other products. Because the OAFlux mixed layers are shallow, they do not entrain the saltier water beneath, and the mixed layers are too fresh (Figure 11f).

[41] The model runs with observed forcing reveal that deep SAMW mixed layer formation can be considered a one-dimensional process; all of the flux products produce mixed layers resembling SAMW in the one-dimensional model. This result does not preclude the potential for advective processes, especially cross-frontal fluxes, to contribute to the deep mixed layers. The contributions of cross-frontal fluxes to creating the observed zonal variation in SAMW mixed layer properties is described by Holte et al. (manuscript in preparation, 2012). Buoyancy loss and wind
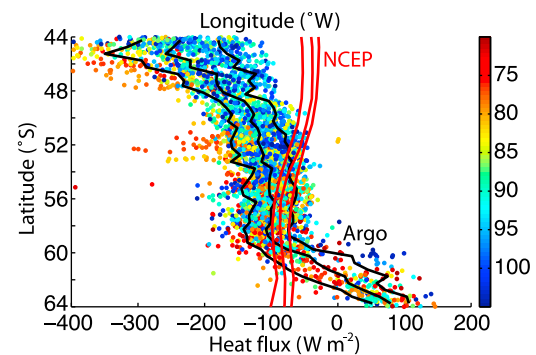

Figure 13. Scaled heat content of Argo profiles (colored circles) collected between January and April plotted as a function of latitude. The heat content is scaled to represent the heat flux necessary to erode the summer profiles into winter profiles with 500 m MLDs by the end of August. The color corresponds to profile longitude. The mean Argo heat flux (± 1 standard deviation) binned by latitude is also plotted (black lines). The mean total NCEP heat flux (± 1 standard deviation) averaged from March to August is plotted in red. The mean NCEP flux was calculated over the region from 105° to 70°W and 44° to 64°S.
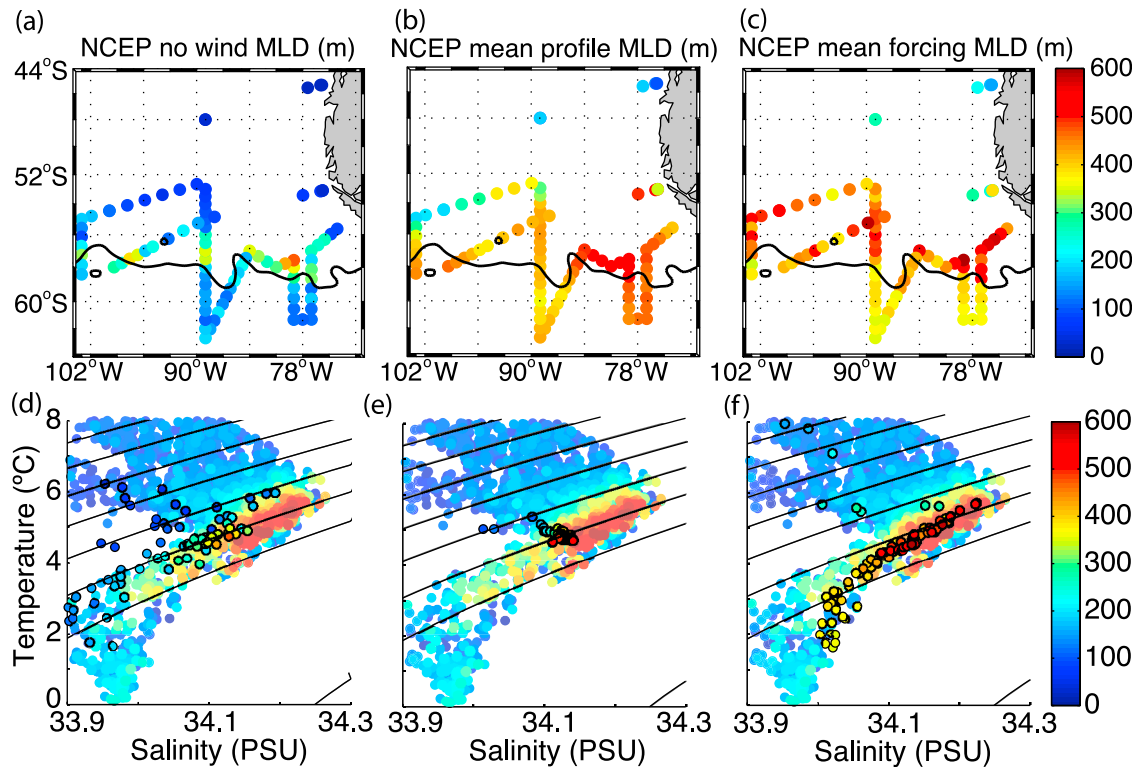
Figure 14. MLD maps and temperature-salinity diagrams of simulated winters for three alternative configurations of KPP run with NCEP forcing: (a, d) no wind, (b, e) mean initial profile (but different forcing), and (c, f) mean forcing (but different initial profiles). The mean profile in Figures 14b and 14e is derived from seven profiles north of the SAF along 89°W (green profiles in Figure 16). In Figures 14c and 14f, the forcing is the mean NCEP forcing in the box spanning 54° to 56°S and 90° to 94°W. In Figures 14d, 14e, and 14f the simulated winter mixed layers are denoted by circles with black borders. The mixed layers from winter Argo profiles are denoted by circles with no borders. The potential density is contoured at 0.1 kg m^{-3} intervals from 26.5 to 27.1 kg m^{-3}.

forcing drive mixing that gradually deepens the mixed layer over the course of the year. The process occurs for a wide range of forcing; as expected, stronger forcing produces deeper SAMW mixed layers. These conclusions are supported by Figure 13; the mean NCEP heat fluxes in the SAMW formation region, particularly between 54° and 59°S, are greater than the mean heat flux necessary to evolve many summer Argo profiles into deep winter SAMW mixed layers. None of the simulations capture the full range of SAMW temperature-salinity properties observed by Argo.

7. One-Dimensional Mixed Layer Modeling With Idealized Forcing

[42] To further test the importance of mixing driven by heat fluxes and wind stress, we run a series of three test cases with NCEP forcing: (1) with NCEP heat fluxes and precipitation but without wind stress, (2) with standard NCEP forcing but replacing the initial profiles with a mean profile from the SAMW formation region, and (3) with initial profiles from the 2006 austral summer cruise but forced by spatial-mean NCEP fields from the SAMW formation region (Figure 14). We use NCEP forcing because it produces mixed layers that more closely resembles Argo SAMW observations than ECMWF (Figure 11).

[43] In run 1, when driven only with heat fluxes and no direct wind stress, the model poorly reproduces SAMW (Figures 14a and 14d); only 23 stations produce deep mixed layers, with depths ranging from 250 to 400 m. The standard NCEP run, with buoyancy and wind forcing, produces more than 20 runs with SAMW mixed layers deeper than 450 m. From this we conclude that wind-driven mixing is essential for forming SAMW mixed layers, at least to the extent that SAMW formation can be explained by one-dimensional mixed layer processes. This result supports the findings of *Sloyan et al.* [2010] and *Kamenkovich* [2005].

[44] Run 2 is initialized with a mean profile. The mean profile is calculated by averaging seven 2006 austral summer CTD profiles collected in the SAMW formation region at CTD depth levels; the profiles are highlighted in green in Figure 12d. This run illuminates the effect of variable forcing on SAMW (Figures 14b and 14e). In the cruise's northwestern section, where the NCEP heat flux is smaller, the simulated SAMW mixed layers are shallower than for the cruise's eastern section, where the heat flux is larger. An annual mean heat flux difference of approximately −30 W m^{-2} results in winter SAMW MLDs that differ by 200 m. The western SAMW MLDs in this test case are deeper than the MLDs in Figure 10b. This test run fails to capture any of the SAMW property variability observed
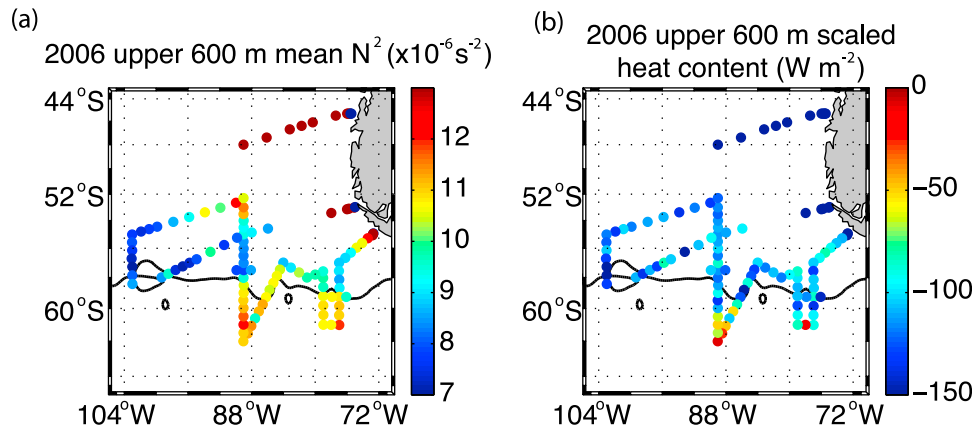
Figure 15. Maps of (a) average N^2 and (b) scaled heat content of the upper 600 m for the 2006 austral summer cruise CTD profiles. The heat content is scaled to represent the average heat flux that would homogenize the profile to a depth of 600 m over 200 days. The mean AVISO dynamic topography contour that most closely matched the SAF location in hydrography and ADCP data is also plotted (black line).

by Argo, as the simulated SAMW properties are all clustered around the initial profile's temperature-salinity properties (Figure 14e). The variable forcing is not strong enough to replicate the observed range of SAMW properties. Therefore the initial profile, and any preconditioning processes, are important in determining the final SAMW mixed layer depths and properties.

[45] Likewise, in run 3 we apply mean forcing, both heat fluxes and wind stress, to all of the actual profiles and the SAMW formation is much more extensive, especially in the cruise's western sections (Figure 14c). The mean forcing is calculated as the spatial average of the NCEP fields in the box spanning 54°S to 56°S and 90°W to 94°W. With this forcing, the simulated SAMW mirrors the full range of SAMW temperature-salinity properties as observed by Argo (Figure 14f). Applying spatial-mean forcing strengthens the forcing in the cruise's western sections, deepening those mixed layers and filling out the temperature-salinity characteristics of the SAMW. In this way, forcing strength indirectly determines the winter SAMW properties by controlling where and how deeply the profiles mix.

8. Importance of Preconditioning to SAMW Formation

[46] The above analysis shows that air-sea fluxes of heat and momentum are important for deepening the SAMW mixed layers. We now look at how the initial summer profile both determines the temperature-salinity characteristics of the final winter SAMW and can also limit the extent of the deepening.

[47] The 2006 austral summer cruise profiles in the SAMW formation region were characterized by low mean stratification in the upper 600 m, generally less than $1 \times 10^{-5} \text{ s}^{-2}$ (Figure 15a). The lowest stratifications were found in the western section of the cruise, which was slightly unexpected, given that the deepest winter mixed layers were found in the eastern sections of the 2005 austral winter cruise, as were the deepest simulated winter SAMW mixed layers, even in the case with mean forcing (Figure 14c).

Summer profiles from the cruise and Argo have high mean stratification in the east because they have very warm, fresh, and shallow mixed layers in the summer (Figure 16). Runoff contributes to the summer low surface salinities in profiles near Chile's coast.

[48] The heat content of the summer profiles is also important, as this heat must be removed for the profiles to mix deeply in the winter. To allow an approximate comparison with observed heat fluxes, we scale the heat content to represent the average heat flux that would homogenize the profiles to a depth of 600 m over 200 days. Summer CTD profiles in the eastern SAMW formation region had less heat stored in the upper 600 m than profiles farther to the west (Figure 15b). We evaluate equation (1) to calculate the contributions of heat flux and evaporation/precipitation to the buoyancy; from March to August, the heat flux contribution (which removes buoyancy) is approximately 5 times larger than that of evaporation/precipitation (which adds buoyancy). With such strong heat fluxes (relative to evaporation/precipitation), we might expect that the heat content of summer profiles would be be an important factor in determining the depth of winter mixed layers.

[49] This pattern of heat storage carries over into the Argo data. Mean upstream profiles from the cruise and Argo exhibit much more salinity structure in the upper 600 m than downstream profiles (Figure 16). Profiles from the west have a subsurface salinity maximum at about 400 m depth, but this feature erodes downstream. This salinity change is accompanied by a downstream decrease in temperature between 100 and 400 m, making downstream profiles denser at depths between 100 and 400 m relative to upstream profiles. This structure promotes the formation of deep mixed layers in the eastern profiles because there is less heat to remove at depth during fall and winter. A low summer heat content alone does not ensure a deep winter mixed layer; the winter forcing must be strong enough to remove the summer mixed layer stratification. In this way, variations in forcing strength do contribute to each winters' expression of the SAMW mixed layers by controlling where and how deeply the SAMW mixes.
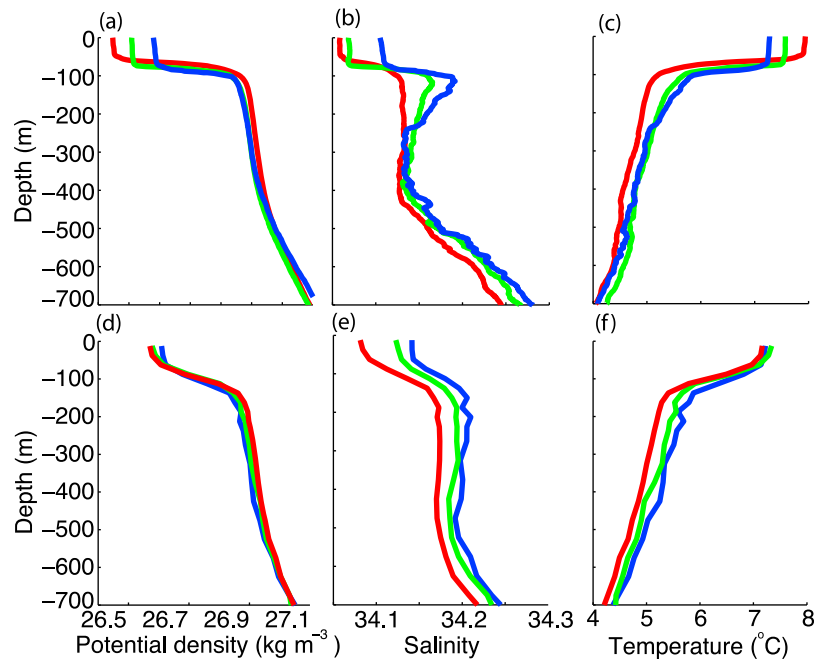
Figure 16. Mean (a) potential density, (b) salinity, and (c) potential temperature profiles for the three groups of CTD profiles from the 2006 austral summer cruise highlighted in Figure 12a. The red profile is composed of profiles from cruise's eastern sector, near 78°W, green represents profiles collected along 89°W, and blue composed of profiles from the west, near 103°W. These profiles all formed deep simulated SAMW winter mixed layers in the NCEP KPP run. Similar mean Argo profiles of mean (d) potential density, (e) salinity, and (f) potential temperature for January, February, and March are calculated for each of the colored boxed regions near each station group in Figure 12a.

[50] Many processes could contribute to the stratification and downstream reduction in heat content. *Sloyan et al.* [2010] indicate that wind mixing, particularly in summer to early autumn, when heat and precipitation fluxes stabilize the water colum, creates the buoyancy difference between east and west. *Sallée et al.* [2010], in estimating Southern Ocean mass exchange between the surface layer and the interior, find that substantial eddy-induced and Ekman transports of nearly 30 Sv approximately counterbalance in the surface layer. Cold core eddies were observed in the SAMW formation region during the cruises, and these eddies could potentially disperse polar waters in the SAMW formation region, reducing the stratification and heat content. Cross-frontal exchange and its contribution to SAMW formation is examined by Holte et al. (manuscript in preparation, 2012).

9. Discussion and Conclusion

[51] This paper examines how air-sea forcing, initial profile stratification, and vertical mixing determine the SAMW mixed layers' depths, properties, area extent, relationship to the SAF, and downstream variation in the southeast Pacific. Using primarily observations from two cruises in the southeast Pacific and a one-dimensional model, we have shown that mixing driven by buoyancy loss and wind forcing is strong enough to deepen the SAMW layers, supporting the findings of *Wang and Matear* [2001]. *Sloyan et al.* [2010] found that wind-driven interior mixing reduced ocean stratification during austral summer and autumn,

preconditioning the water column for the rapid formation of deep SAMW mixed layers during winter. In their Southern Ocean heat budget, *Dong et al.* [2007] found that the mixed layer temperature seasonal cycle was most likely attributable to air-sea heat fluxes. *Dong et al.* [2008] noted that the heat loss to the atmosphere in the eastern Pacific was stronger than that in the Indian Ocean, suggesting that air-sea heat exchange may play a relatively larger role in SAMW formation in the eastern Pacific than in other oceans. Cross-frontal processes are apparently not necessary for deepening the SAMW mixed layers in winter, though Holte et al. (manuscript in preparation, 2012) find that the cross-frontal exchange diagnosed by an OMP analysis is consistent with the along-front freshening and cooling of the SAMW mixed layers observed by Argo. Cross-frontal exchange in the form of Ekman transport, eddies, and intrusions is therefore likely important in setting SAMW properties.

[52] Our work builds on previous studies by demonstrating how air-sea fluxes and initial profile combine to determine the locations of SAMW formation, as well as the SAMW properties. The air-sea fluxes only effect small property changes in SAMW, as found by *Speer et al.* [2000] and *Sloyan and Rintoul* [2001], but forcing strength indirectly influences the winter SAMW properties by controlling how deeply the profiles mix. The stratification and heat content of the initial profiles are important in determining the properties of the SAMW and the likelihood of deep mixing. Highly stratified profiles with large heat storage are less likely to form deep SAMW mixed layers. In contrast,

the summer profiles just upstream of Drake Passage have less heat stored between 100 and 600 m than profiles from farther upstream, and so, with sufficiently strong winter forcing, form a cold, dense variety of SAMW. Therefore, any atmospheric mode, such as El Niño–Southern Oscillation or Southern Annular Mode, that alters air-sea fluxes in the southeast Pacific could change SAMW properties, supporting the results of *Naveira-Garabato et al.* [2009] and *Vivier et al.* [2010].

[53] Our results suggest that accurate ocean structure and air-sea fluxes are very important for producing accurate SAMW in models. Any processes that contribute to setting the ocean structure (stratification and heat content), including lateral processes, would be important for successful modeling of SAMW formation.

References

Albérola, C., C. Millot, U. Send, C. Mertens, and J.-L. Fuda (1996), Comparison of XCTD/CTD data, *Deep Sea Res. Part I*, 43, 859–876.
Banks, H. T., R. A. Wood, J. M. Gregory, T. C. Johns, and G. S. Jones (2000), Are observed decadal changes in Intermediate Water masses a signature of anthropogenic climate change?, *Geophys. Res. Lett.*, 27, 2961–2964, doi:10.1029/2000GL011601.
Bryden, H. L., E. L. McDonagh, and B. A. King (2003), Changes in ocean water mass properties: Oscillations or trends? *Science*, 300, 2086–2089.
Cerovecki, I., L. Talley, and M. Mazloff (2011), A comparison of Southern Ocean air-sea buoyancy flux from an ocean state estimate with five other products, *J. Clim.*, 24, 6283–6306.
Chereskin, T. K., L. D. Talley, and B. M. Sloyan (2010), Nonlinear vorticity balance of the Subantarctic Front in the southeast Pacific, *J. Geophys. Res.*, 115, C06026, doi:10.1029/2009JC005611.
Dong, S., S. T. Gille, and J. Sprintall (2007), An assessment of the Southern Ocean mixed layer heat budget, *J. Clim.*, 20, 4425–4442.
Dong, S., J. Sprintall, S. T. Gille, and L. Talley (2008), Southern Ocean mixed-layer depth from Argo float profiles, *J. Geophys. Res.*, 113, C06013, doi:10.1029/2006JC004051.
Fairall, C. W., E. F. Bradley, J. E. Hare, A. A. Grachev, and J. B. Edson (2003), Bulk parameterization of air-sea fluxes: Updates and verification for the COARE algorithm, *J. Clim.*, 16, 571–591.
Gille, S. T. (2002), Warming of the Southern Ocean since the 1950s, *Science*, 295, 1275–1278.
Hanawa, K., and L. D. Talley (2001), Mode Waters, in *Ocean Circulation and Climate: Observing and Modelling the Global Ocean*, edited by G. Siedler, J. Church, and J. Gould, pp. 373–386, Academic, London.
Hartin, C., R. Fine, B. Sloyan, L. Talley, and J. Happell (2011), Formation rates of Subantarctic Mode Water and Antarctic Intermediate Water within the South Pacific, *Deep Sea Res. Part I*, 58, 524–534.
Herraiz-Borreguero, L., and S. R. Rintoul (2010), Subantarctic Mode Water variability influenced by mesoscale eddies south of Tasmania, *J. Geophys. Res.*, 115, C04004, doi:10.1029/2008JC005146.
Hogg, A. M. C., M. P. Meredith, J. R. Blundell, and C. Wilson (2008), Eddy heat flux in the Southern Ocean: Response to variable wind forcing, *J. Clim.*, 21, 608–620.
Holte, J., and L. Talley (2009), A new algorithm for finding mixed layer depths with applications to Argo data and Subantarctic Mode Water formation, *J. Atmos. Oceanic Technol.*, 26, 1920–1939.
Joyce, T. M., L. N. Thomas, and F. Bahr (2009), Wintertime observations of Subtropical Mode Water formation within the Gulf Stream, *Geophys. Res. Lett.*, 36, L02607, doi:10.1029/2008GL035918.

Kalnay, E., et al. (1996), The NCEP/NCAR 40-year reanalysis project, *Bull. Am. Meteorol. Soc.*, 77, 437–472.
Kamenkovich, I. V. (2005), Role of daily surface forcing in setting the temperature and mixed layer structure of the Southern Ocean, *J. Geophys. Res.*, 110, C07006, doi:10.1029/2004JC002610.
Kantha, L., and C. Clayson (1994), *Numerical Models of Oceans and Oceanic Processes*, *Int. Geophys. Ser.*, vol. 66, 940 pp., Academic, San Diego, Calif.
Keeling, R. F., and B. B. Stephens (2001), Antarctic sea ice and the control of Pleistocene climate instability, *Paleoceanography*, 16, 112–131, doi:10.1029/2000PA000529.
Kelly, K. A., S. Dickinson, and Z. Yu (1999), NSCAT tropical wind stress maps: Implications for improving ocean modeling, *J. Geophys. Res.*, 104, 11,291–11,310, doi:10.1029/1998JC900036.
Large, W. G., J. C. McWilliams, and S. C. Doney (1994), Oceanic vertical mixing: A review and a model with a nonlocal boundary layer parameterization, *Rev. Geophys.*, 32, 363–404, doi:10.1029/94RG01872.
Mazloff, M. R., P. Heimbach, and C. Wunsch (2010), An eddy-permitting Southern Ocean state estimate, *J. Phys. Oceanogr.*, 40, 880–899.
McCartney, M. S. (1977), Subantarctic Mode Water, in *A Voyage of Discovery: George Deacon 70th Anniversary Volume*, edited by M. V. Angel, pp. 103–119, Pergamon, Oxford, U. K.
McCartney, M. S. (1982), The subtropical recirculation of mode waters, *J. Mar. Res.*, 24, 427–464.
Mellor, G. L., and T. Yamada (1982), Development of a turbulence closure model for geophysical fluid problems, *Rev. Geophys.*, 20, 851–875, doi:10.1029/RG020i004p00851.
Naveira-Garabato, A. C., L. Jullion, D. P. Stevens, K. J. Heywood, and B. A. King (2009), Variability of Subantarctic Mode Water and Antarctic Intermediate Water in the Drake Passage during the late-twentieth and early-twenty-first centuries, *J. Clim.*, 22, 3661–3688.
Pahnke, K., and R. Zahn (2005), Southern Hemisphere water mass conversion linked with North Atlantic climate variability, *Science*, 307, 1741–1746.
Park, Y., and L. Gambéroni (1997), Cross-frontal exchange of Antarctic Intermediate Water and Antarctic Bottom Water in the Crozet Basin, *Deep Sea Res. Part II*, 44, 963–986.
Price, J. F., R. A. Weller, and R. Pinkel (1986), Diurnal cycling: Observations and models of the upper ocean response to diurnal heating, cooling, and wind mixing, *J. Geophys. Res.*, 91, 8411–8427.
Ren, L., K. Speer, and E. P. Chassignet (2011), The mixed layer salinity budget and sea ice in the Southern Ocean, *J. Geophys. Res.*, 116, C08031, doi:10.1029/2010JC006634.
Rintoul, S., and M. England (2002), Ekman transport dominates local air-sea fluxes in driving variability of Subantarctic Mode Water, *J. Phys. Oceanogr.*, 32, 1308–1321.
Sabine, C. L., R. A. Feely, R. M. Key, J. L. Bullister, F. J. Millero, K. Lee, T.-H. Peng, B. Tilbrook, T. Ono, and C. S. Wong (2002), Distribution of anthropogenic CO$_2$ in the Pacific Ocean, *Global Biogeochem. Cycles*, 16(4), 1083, doi:10.1029/2001GB001639.
Sallée, J.-B., R. Morrow, and K. Speer (2008), Eddy heat diffusion and Subantarctic Mode Water formation, *Geophys. Res. Lett.*, 35, L05607, doi:10.1029/2007GL032827.
Sallée, J.-B., K. Speer, S. Rintoul, and S. Wijffels (2010), Southern Ocean thermocline ventilation, *J. Phys. Oceanogr.*, 40, 509–529.
Sathiyamoorthy, S., and G. W. K. Moore (2002), Buoyancy flux at Ocean Station Bravo, *J. Phys. Oceanogr.*, 32, 458–474.
Sloyan, B., and S. Rintoul (2001), Circulation, renewal, and modification of Antarctic Mode and Intermediate Water, *J. Phys. Oceanogr.*, 31, 1005–1030.
Sloyan, B., L. Talley, T. Chereskin, R. Fine, and J. Holte (2010), Antarctic Intermediate Water and Subantarctic Mode Water formation in the southeast Pacific: The role of turbulent mixing, *J. Phys. Oceanogr.*, 40, 1558–1574.
Speer, K., S. Rintoul, and B. Sloyan (2000), The diabatic Deacon cell, *J. Phys. Oceanogr.*, 30, 3212–3222.
Talley, L. D. (1996), Antarctic Intermediate Water in the South Atlantic, in *The South Atlantic: Present and Past Circulation*, edited by G. Wefer et al., pp. 219–238, Springer, Berlin.
Talley, L. D., V. Lobanov, V. Ponomarev, A. Salyuk, P. Tishchenko, I. Zhabin, and S. Riser (2003), Deep convection and brine rejection in the Japan Sea, *Geophys. Res. Lett.*, 30(4), 1159, doi:10.1029/2002GL016451.
Vivier, F., D. Iudicone, F. Busdraghi, and Y.-H. Park (2010), Dynamics of sea-surface temperature anomalies in the Southern Ocean diagnosed from a 2D mixed-layer model, *Clim. Dyn.*, 34, 153–184.
Wang, X., and R. J. Matear (2001), Modeling the upper ocean dynamics in the Subantarctic and Polar Frontal Zones in the Australian sector of the

Southern Ocean, *J. Geophys. Res.*, *106*, 31,511–31,524, doi:10.1029/2000JC000357.

Wong, A. P. S., N. L. Bindoff, and J. A. Church (2001), Freshwater and heat changes in the North and South Pacific Oceans between the 1960s and 1985–94, *J. Clim.*, *14*, 1613–1633.

Yu, L., X. Jin, and R. A. Weller (2008), Multidecade global flux datasets from the Objectively Analyzed Air-sea Fluxes (OAFlux) project: Latent and sensible heat fluxes, ocean evaporation, and related surface meteorological variables, *OAFlux Proj. Tech. Rep. OA-2008-01*, 64 pp., Woods Hole Oceanogr. Inst., Woods Hole, Mass.

Yuter, S. E., and W. S. Parker (2001), Rainfall measurement on ship revisited: The 1997 PACS TEPPS cruise, *J. Appl. Meteorol.*, *40*, 1003–1018.

T. K. Chereskin and L. D. Talley, Scripps Institution of Oceanography, University of California, San Diego, 9500 Gilman Dr., La Jolla, CA 92093-0230, USA.

J. W. Holte, Woods Hole Oceanographic Institution, 266 Woods Hole Rd., MS 21, Woods Hole, MA 02543, USA. (jholte@whoi.edu)

B. M. Sloyan, Center for Australian Weather and Climate Research, CSIRO Marine and Atmospheric Research, GPO 1583, Hobart, Tas 7001, Australia.